Charge exchange, excitation, and ionization in A^{Z+}+H(1s) collisions in strong magnetic fields

B. He,[1] J. G. Wang,[1] and R. K. Janev[2]

[1]*Key Laboratory of Computational Physics, Institute of Applied Physics and Computational Mathematics,
Beijing 100088, People's Republic of China*
[2]*Macedonian Academy of Sciences and Arts, P.O.B. 428, 1000 Skopje, Macedonia*

The effects of strong magnetic fields ($B \sim 10^4$ T) on charge exchange, excitation, and ionization processes in collisions of H(1s) atoms with fully stripped ions A^{Z+} are studied by the classical trajectory Monte Carlo method in the energy range 25–2000 keV/u. The cases $\vec{B} \| \vec{v}$ and $\vec{B} \perp \vec{v}$, where $\vec{v}$ is the velocity vector of A^{Z+} ion, are considered. It was found that in the considered energy range and for $B \leq 5 \times 10^4$ T and $Z=2,6$, the parallel magnetic field insignificantly affects the charge exchange cross section, but leads to an increase of excitation and ionization cross sections in the region below 100–200 keV/u (up to a factor of 1.5–4 at 25 keV/u for $Z=2$ and 6, respectively). The transverse magnetic field, however, causes a significant (up to a factor of 4) reduction of total charge exchange cross section in the entire energy range investigated and to a dramatic increase of excitation and ionization cross sections (up to one to two orders of magnitude for $Z=2$ and 6, respectively, at $E \sim 25$ keV/u and $B=5 \times 10^4$ T). The physics of magnetic field effects on considered processes is analyzed in terms of time evolution of interactions in the system, total electron energy, and electron trajectories. It was found that the major effects induced by the magnetic field are associated with the diamagnetic term in the interaction, continuum electron trapping in the projectile or target regions, and the Lorentz force. The energy distributions of captured and ionized electrons, as well as the momentum distributions of ionized electrons are also studied.

PACS number(s): 34.50.Fa, 34.70.+e

I. INTRODUCTION

The atomic collision processes in strong external magnetic fields have been subject to significant interest in the last several decades, the motivation coming from potentially important applications in astrophysics where magnetic fields as strong as 10^2–10^5 T (white dwarfs), and even 10^7–10^9 T (neutron stars) have been found. The strong external magnetic field affects both the electronic structure of colliding system [regarded as two individual colliding atoms or ions (see, e.g., Refs. [1,2])], or as a quasimolecule (see, e.g., Refs. [3–5]) and its collision dynamics. In the studies of magnetic field effects on the structure and dynamics of atomic systems, it is convenient to measure the strength of magnetic field B in terms of the parameter $\gamma = B/B_0$, where $B_0 = 2.3505 \times 10^5$ T is the field for which the electron-cyclotron frequency $eB/m_0 c$ is equal to the atomic unit of frequency $m_0 e^4/\hbar^3$. Most of the atomic collision studies involving heavy particles in external magnetic fields have been performed for the electron capture process in one- or quasi-one-electron collision systems and for fields significantly smaller than $B_0(\gamma \ll 1)$ to avoid a significant perturbation of the electronic structure.

The manifestation of the effects of magnetic field on the collision dynamics depends, to a certain degree, on the theoretical framework within which the dynamics is described. The first study of the effects of an external homogeneous magnetic field on ion-atom collision processes was performed for the resonant electron capture in H$^+$+H(1s) and Rb$^+$+Rb collision systems for $\gamma \leq 0.05$ and collision energies below 200 keV/u by employing the atomic orbital close-coupling (AOCC) method with a two-state basis [6]. It was found that the magnetic field significantly reduces the cap-

ture cross section in this energy range (up to 43% for Rb$^+$+Rb at $\gamma = 0.05$ and a collision velocity $v = 6.8 \times 10^6$ cm/s). In another five-state AOCC study of the electron capture in the He^{2+}+H(1s) collision system, performed in the energy range 6.25–400 keV/u for $\gamma \leq 0.2$ [7], the cross section reduction was found to be rather modest, ranging from 8% at $E = 6.25$ keV/u to 0% at 100 keV/u for $\gamma = 0.2$. For energies above ~ 100 keV/u, even a slight increase of the total electron capture cross section was observed (about 1% at $E = 400$ keV/u). In both these studies, the orientation of external magnetic field was parallel to the projectile ion velocity vector.

A molecular orbital close-coupling (MOCC) study, with a two-state basis, of the resonant electron exchange process in the H$^+$+H(1s) system was performed in Ref. [8] for collision energies below 25 keV/u and field strengths up to $\gamma = 1$. The Schrödinger equation with the Born-Oppenheimer Hamiltonian including the external field was solved to determine the "magnetically dressed" $1s\sigma_u$ and $1s\sigma_g$ orbitals and their energies. It was found that the electron capture cross section in the presence of magnetic field decreases by a factor of 3.4 at $E = 1$ keV/u, $\gamma = 1$ and by a factor of 2.3 at $E = 25$ keV/u, $\gamma = 1$, with respect to that in the field-free case. However, in another MOCC study of the electron capture in the B^{4+}+H(1s) system [9], performed in the energy region below 250 keV/u with $\gamma \leq 0.05$ and using 13 coupled MOs, it was found that the total capture cross section increases with increasing γ (up to 33% for $E = 122.5$ keV/u and $\gamma = 0.05$) with respect to that of field-free case.

The differences in the role of magnetic field in the electron capture dynamics in different collision systems and for different energies results from the interplay of four major factors introduced by the field: removal of Coulomb degen-

eracy of one electron system (Zeeman splitting), diamagnetic shift of the energy levels, change of the dynamical couplings and change of the relative phase between the initial and final wave functions (which arises if the gauge of the magnetic vector potential is properly referred to one and the same origin throughout the collision [6,8]). For instance, while at low collision energies the relative phase factor dominantly affects the capture dynamics [6], its role at high energies becomes insignificant compared to the electron momentum transfer phase factor (see, e.g., Ref. [7]).

The classical trajectory Monte Carlo (CTMC) method has also been used to study the electron capture and ionization processes in $He^{2+}+H(1s)$ system [10] for $\gamma \lesssim 0.2$ and $E = 25$, 50 and 75 keV/u, with the orientation of the magnetic field parallel to the relative velocity vector $\vec{B} \| \vec{v}$. The cross section calculations were performed with only 6000 trajectories, producing standard errors of the result of 10–20 %. With this uncertainty, no significant variations of the total charge exchange and ionization cross sections for the selected three energies and $\gamma \lesssim 0.2$ were observed with respect to their field-free values. In a more recent work [11,12], the CTMC method was used to study the electron capture and ionization processes in collisions of Rydberg atoms (with principal quantum number $n=28$) with singly charged ions in an external field of 4 T (the corresponding values of parameter γ being ≈ 0.1) at collision energies 1.3–130 eV/u (reduced collision velocity $v_r = vn = 0.2$–2.0 a.u.). Based on the results of quantum and classical perturbation theories of the Rydberg atom in an external magnetic field, developed in Refs. [13,14], respectively, the authors of Refs. [11,12] were able to construct the classical microcanonical distributions for the magnetically split (and energetically shifted) angular states of the nth manifold, characterized by the quasimomentum K. However, the cross section calculations were performed only for the states with the extreme values of K, when the radial electron distribution is either strongly elongated in the direction of magnetic field ($K=K_{max}$), or has a disklike form perpendicular to the field direction ($K=K_{min}$). With respect to the field-free CTMC cross sections for electron capture (σ_{cx}^0) and ionization (σ_i^0) for the $n=28$, $l=2$, $m=0$ state, the ionization cross section in presence of the magnetic field (σ_i^B) is larger than σ_i^0 for $v_r < 1$ a.u. and smaller than σ_i^0 for $v_r > 1$ a.u. for both K_{max} and K_{min}. On the other hand, while for K_{min} the electron capture cross section σ_{cx}^B is smaller than σ_{cx}^0 in the entire velocity range investigated (by a factor of 2 for $v_r \approx 0.5$ a.u.), σ_{cx}^B for K_{max} is smaller (significantly) than σ_{cx}^0 for $v_r \lesssim 0.8$ a.u., but larger than σ_{cx}^0 at higher velocities. While these results can be helpful to infer the effect of magnetic field on σ_i for a broader range of v_r, and on σ_{cx} for $v_r \lesssim 1$, they are insufficient to make any conclusive judgment about the values for σ_{cx}^B relative to σ_{cx}^0. We note that the study in Refs. [11,12] was also performed for the $\vec{B} \| \vec{v}$ case. Within the same extended CTMC method an extensive study has been performed in Ref. [15] of the ionization process in ion—Rydberg atom collisions in the $\vec{B} \| \vec{v}$ case with particular attention to the ionization mechanisms and velocity distribution of emitted electrons.

In the present article we shall undertake a more detailed study of processes (A^{Z+} is a completely stripped ion)

$$A^{Z+} + H(1s) \rightarrow A^{(Z-1)} + H^+, \tag{1}$$

$$\rightarrow A^{Z+} + H^*, \tag{2}$$

$$\rightarrow A^{Z+} + H^+ + e \tag{3}$$

in an external magnetic field by employing the CTMC method. We shall consider both $\vec{B} \| \vec{v}$ and $\vec{B} \perp \vec{v}$ cases, the later of which has not received much attention so far. The appearance of the Lorentz force in the $\vec{B} \perp \vec{v}$ case makes the collision dynamics of processes (1)–(3) more complex, facilitating in particular the channel (3) (Lorentz ionization; see, e.g., Ref. [16]). The diamagnetic term in the interaction potential forms a parabolic potential well along the direction of external magnetic field confining the electron trajectories in the perpendicular direction. This has a significant effect on the spectra of emitted electrons in the ionization process and on the electron capture dynamics in the transverse magnetic field. In order to gain an insight into the dynamics of processes (1)–(3) we shall analyze the time evolution of interactions in the system, total electron energy and electron distances from the target proton and the projectile. Most of the study will concentrate on the case of $Z=2$ ion, but cross section calculations will also be performed for the $Z=6$ ion to see the influence of magnetic field on the known Z-scaling properties of the total cross sections of reactions (1)–(3) [17].

The article is organized as follows. In the next section we give a brief account of the computational method. In Sec. III, we present the results of calculations for the total cross sections of reactions (1)–(3) for both $\vec{B} \| \vec{v}$ and the $\vec{B} \perp \vec{v}$ cases and analyze their relative magnitudes in terms of the magnetic terms in the interaction potential. In Sec. IV, we analyze the electron capture, excitation, and ionization processes in terms of time evolution of electron trajectories, with special attention to the underlying dynamical mechanisms. In Sec. V we present and discuss the results on energy distributions of captured, excited and emitted electrons in processes (1)–(3), as well as the velocity distributions of emitted electrons. Finally, in Sec. VI we give our conclusions. Atomic units ($e=m_e=\hbar=1$) will be used in this work unless otherwise explicitly indicated.

II. FORMULATION OF THE PROBLEM AND COMPUTATIONAL METHOD

The CMTC method (see, e.g., Refs. [18,19]), for description of three-body collision dynamics has widely been used in electron and ion atom collision physics. It proved to provide an adequate description of the collision dynamics in the energy region where many coupled states are involved [e.g., for relative collision velocities $v \sim (0.5-3)v_0$ in the case of heavy particle collisions, where v_0 is the classical velocity of the initial state bound electron]. The formulation of CTMC method for the three charged-particle dynamics in an external homogeneous magnetic field B, within the symmetric Coulomb gauge for the magnetic vector potential $[\vec{A}(\vec{r}) = \frac{1}{2}\vec{B} \times \vec{r}]$, was given in Ref. [10], including the derivation of CTMC equations for the case when one of the particles is

much lighter (electron) than the other two (ions) and when the condition $\gamma \ll 1$ is fulfilled. In this approximation the three-body center-of-mass is moving uniformly and the magnetic field affects only the motion of the light particle. A further approximation of CTMC equations for ion-atom collisions is usually made by adopting the straight-line trajectory approximation for the motion of the projectile (ion) with respect to the target (atom), which is a justifiable approximation in the energy range of validity of the CTMC method.

A nontrivial aspect in the application of CTMC method to the $A^{Z+}+H(1s)$ collision dynamics in an external magnetic field is the question of the effect of the field on the microcanonical distribution (ensemble of Kepler orbits) representing the electron initial state [18]. For magnetic field strengths below $\gamma = 0.2$, the magnetic shift of the energy of $H(1s)$ state is smaller than 2% (see, e.g. Refs. [2,7]) and, as argued in Ref. [10], the electron wave function is only weakly perturbed by such fields. This means that for $\gamma \leq 0.2$ the classical electron momentum distribution remains close to the quantum-mechanical one [18]. Restricting our study of processes (1)–(3) to fields with $\gamma \leq 0.2$, and adopting the field-free microcanonical distribution to represent the initial electron state, the magnetic field effects in the dynamics of these processes can be investigated on a direct way. We should mention, however, that the $\gamma \ll 1$ restriction of the use of CTMC method to one-electron ion-atom collision systems can be removed by the recently developed procedure for determining the classical initial state microcanonical distribution of a bound atomic state in the presence of magnetic fields of considerably higher strength [11,12].

When solving the CTMC equations, we place the origin of the coordinate system at the position of the proton of the $H(1s)$ atom and then the initial conditions for the electron coordinates and momenta are defined by the above mentioned field-free microcanonical distribution. The initial conditions for the projectile A^{Z+} in this reference frame are specified by its velocity $\vec{v}$, its impact parameter $\vec{b}(\perp \vec{v})$, and its initial distance R_{pt}^0 from the target. We choose the z axis of our reference frame along the direction of $\vec{v}$. To reproduce a uniform flux of particles with a fixed velocity vector $\vec{v}$, the impact parameter value is selected randomly from the interval $[0, b_{max}]$, where b_{max} is sufficiently large that for $b > b_{max}$ the probability of inelastic processes in $A^{Z+}+H(1s)$ system is negligible. The value of the b_{max} depends on both Z and v. The distance R_{pt}^0 should be large enough to ensure that the projectile-proton and electron-projectile interaction are negligible with respect to electron-proton interaction. Since for a fixed projectile velocity (and R_{pt}^0 distance) the impact parameter values are chosen randomly from the interval $[0, b_{max}]$, as are the initial electron coordinates and momenta from the microcanonical distribution, to ensure a statistically meaningful result from the solution of classical equations of motion, the number of trajectories should be sufficiently large. In the calculations presented in this paper, the total number of trajectories was taken to be at least 2×10^5. The value of b_{max} for each projectile velocity (and charge) was chosen so as to ensure converged results and to minimize the statistical error (to less than 5%).

The integration of classical (Hamiltonian's) equations of motion is carried out (from the distance R_{pt}^0, when time

$t=0$) up to times when R_{pt} is sufficiently large to ensure that proton-projectile interaction is negligible and the electron is found (judging by its trajectory and total energy) either around the proton, the projectile, or far from each of them. After each Monte Carlo trajectory, the total electron energy relative to the proton (E_{et}) and to the projectile (E_{ep}) is calculated to judge about the result of the collision. When it is found that for a given trajectory both E_{et} and E_{ep} are positive, the event is classified as ionization, when $E_{et}>0$ and $E_{ep}<0$, the event is classified as electron capture, and when $E_{et}<0$ and $E_{ep}>0$, the event is classified as elastic or excitation. When $E_{ep}>0$ and $0>E_{et}>-0.22$ [which correspond to $(-2E_{et})^{-1/2}>1.5$] the event is classified as excitation. The total energies E_{et} and E_{ep}, are defined as $E_{et}=\frac{1}{2}v_e^2-1/r_{et}$ and $E_{ep}=\frac{1}{2}(\vec{v}_e-\vec{v})^2-Z/r_{ep}$, where $\vec{v}_e$ is the electron velocity, $\vec{v}$ is the projectile velocity, and the indices e, p, and t refer to the electron, projectile, and the target proton, respectively.

Information about the quantum states (n,l,m) populated in excitation and electron capture processes (by using the quantum-classical correspondence principle) cannot be extracted from the present CTMC calculations, since in the presence of a magnetic field the total orbital angular momentum l is no longer a conserved quantity (but its component along the field direction is). The presence of Lorentz force in the transverse magnetic field case $\vec{B} \perp \vec{v}$ makes the atomic energy levels quasistationary and the principal quantum number n is no longer a "good" quantum number too. In the next section, we present the total cross sections for reactions (1)–(3), while the corresponding classical energy distributions of excited, ionized, and captured electrons will be given in Sec. V.

III. TOTAL CROSS SECTIONS

We have performed total cross section calculations for the processes (1)–(3) for $Z=2$ and 6 by the CTMC method (using the event classification criteria described in the preceding section) for magnetic fields with $\gamma \leq 0.2$ and orientation both parallel and perpendicular to the ion velocity vector $\vec{v}$. The latter was taken to be oriented along the z-axis and the transverse magnetic field along the x axis. The two cases of orientation of magnetic field with respect to $\vec{v}$ will be indicated by subscripts z and x in γ. The collision energy was varied in the energy range 25–2000 keV/u.

The result of cross section calculations for $Z=2$ for $\gamma_z = 0.2$ and $\gamma_x = 0.05$, 0.1, 0.2 are shown in Figs. 1(a)–1(c) together with the field-free ($\gamma=0.0$) cross sections. For the case of parallel field ($B=B_z$), the total charge exchange cross section shows little dependence on the field strength and, therefore, only the case with $\gamma_z=0.2$ is shown in Fig. 1(a). Its difference from the field-free cross section is statistically insignificant. The effect of parallel magnetic field on the total excitation and ionization cross section for $Z=2$ [Figs. 1(b) and 1(c)] is, however, quite significant for collision energy below $\sim 150–200$ keV/u. These cross sections increase with decreasing the energy and with increasing γ_z. Only the cross sections for $\gamma_z=0.2$, for which the effect is the strongest, are shown in these figures. At $E=25$ keV/u the $B_z=0.2B_0$ field
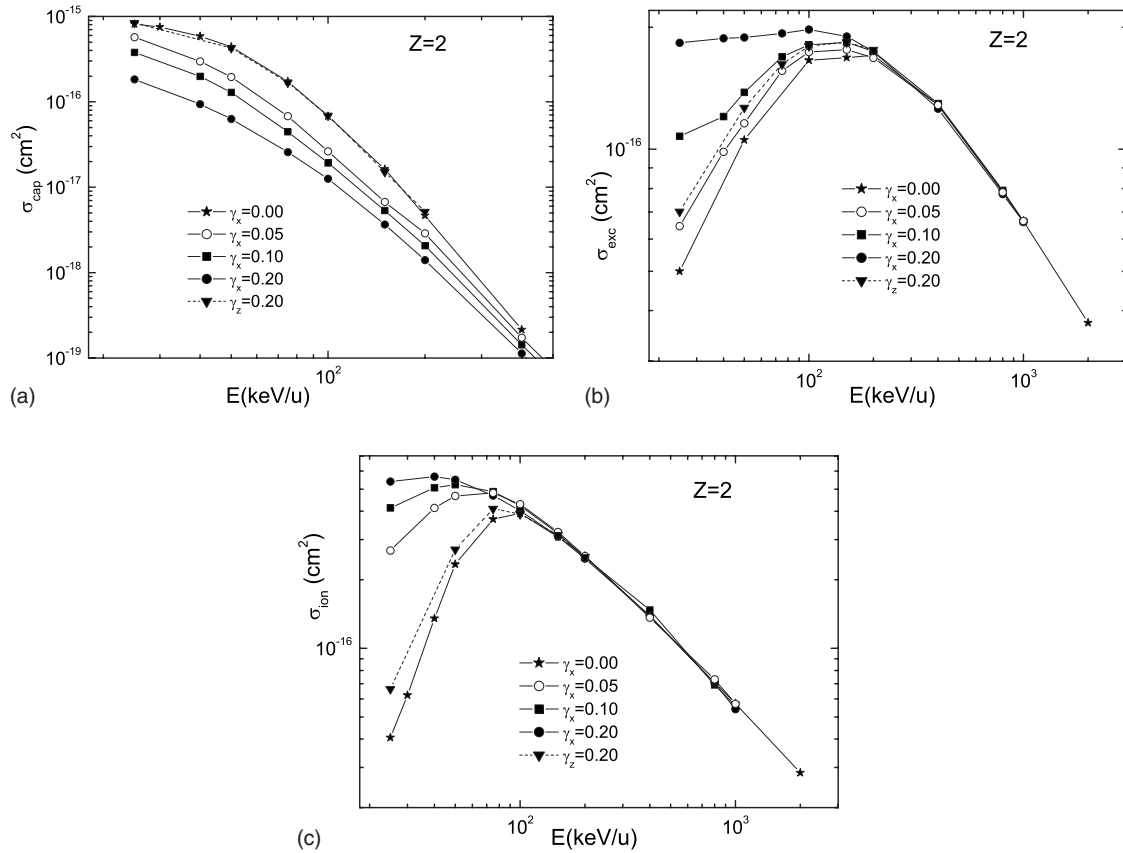
FIG. 1. Total cross sections for electron capture (a), excitation (b), and ionization (c) in He^{2+}+H(1s) collisions in a parallel (γ_z=0.2) and transverse (γ_x=0.05, 0.1, 0.2) external magnetic fields and in the field-free case (γ=0.0).

leads to an increase of total ionization and excitation cross section by a factor of about 1.5.

The changes in the cross sections of Eqs. (1)–(3) for Z =2 induced by the transverse magnetic field B_x are, however, very significant. The charge exchange cross section is progressively reduced with increasing the field strength in the entire energy range investigated, this reduction reaching for γ_x=0.2 a factor of about 4 at E=25 keV/u and a factor about 2 at E=400 keV/u [see Fig. 1(a)]. In contrast to this, the excitation [Fig. 1(b)] and ionization [Fig. 1(c)] cross sections are only slightly increased at energies above $\sim$100 keV/u and $\sim$200 keV/u, respectively, but their increase with increasing γ_x and decreasing the energy below $\sim$100–200 keV/u becomes dramatic (a factor of about 3.5 and 14 for γ_x=0.2 at E=25 keV/u for excitation and ionization, respectively).

The cross sections of processes (1)–(3) for Z=6 are shown in Figs. 2(a)–2(c). The parallel and transverse magnetic fields affect the cross sections of these processes in the same way as in the Z=2 case. The B_z field in this case also has a negligible effect on the charge transfer cross section for γ_z=0.2 in the entire energy range investigated [Fig. 2(a)], but leads to an increase of excitation [Fig. 2(b)] and ionization [Fig. 2(c)] cross sections below $\sim$100 keV/u which is more pronounced than in the Z=2 case. In the case of transverse magnetic field, the cross section changes with respect to the field-free case have the same character as in the Z=2 case but are by far more pronounced. The analysis of the energy

and Z behavior of the cross sections displayed in Figs. 1 and 2 indicates that both the parallel and transverse magnetic fields preserve the general character of the Z and E dependences of the field-free CTMC electron capture cross sections [18]. For the excitation and ionization cross sections the character of these dependences remains the same as in the field-free case only at high energies. In the energy regions below $\sim$100Z keV/u for excitation and below $\sim$50Z keV/u for ionization the inverse dependence of excitation and ionization cross sections on Z in the free-field case (see, e.g., Ref. [18]) is preserved only in the parallel magnetic field. In the transverse magnetic field also the energy dependence of the cross sections for these processes is drastically changed in this energy region (see Figs. 1 and 2).

A qualitative understanding of the changes in the total inelastic cross sections in Figs. 1 and 2 introduced by the external magnetic field can be obtained already from the form of the potential in which the electron motion takes place. The Hamiltonian governing the electron trajectory in the A^{Z+}+H system in an external homogeneous magnetic field $\vec{B}$ is

$$H_{el} = \frac{1}{2}\vec{p}^2 + V(\vec{r}, \vec{R}; \vec{B}), \quad (4)$$

where $\vec{p}$ is the electron momentum and V is its interaction with the target nucleus, projectile, and the magnetic field. With the coordinate origin placed at the target nucleus and a
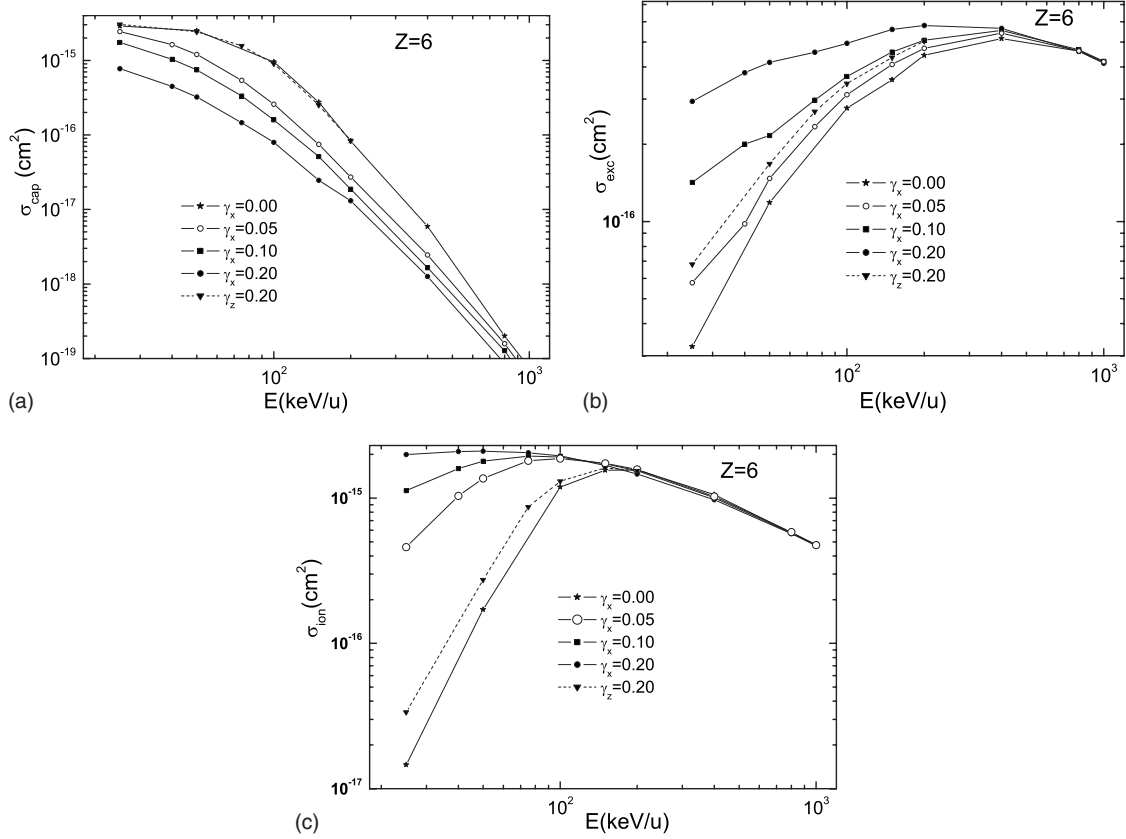
FIG. 2. Same as in Fig. 1, but for the $C^{6+}+H(1s)$ collision.

Coulomb symmetric gauge with respect to target nucleus, the interaction V has the form

$$V(\vec{r},\vec{R};\vec{B}) = -\frac{1}{|\vec{r}|} - \frac{Z}{|\vec{r}-\vec{R}|} + \frac{1}{2}\gamma_\alpha l_\alpha + \frac{1}{8}\gamma_\alpha^2 \rho_{\bar{\alpha}}^2, \qquad (5)$$

where $\vec{r}$ and $\vec{R}$ are the electron and projectile radius vectors with respect to target nucleus, respectively, $\alpha(=z,x)$ indicates the field direction, l_α is the projection of electron angular momentum on the field direction, and $\rho_{\bar{\alpha}}$ is the distance in the direction perpendicular to the field. We take the impact parameter $\vec{b}$ to be oriented along the x direction (the velocity vector $\vec{v}$ in the present study will always be oriented along the z direction) so that

$$|\vec{r}-\vec{R}| = [(b-x)^2 + y^2 + (z-z_0)^2]^{1/2}, \quad z_0 = vt, \qquad (6)$$

where t is the time. In the cases of parallel $(B=B_z)$ and transverse $(B=B_x)$ fields the diamagnetic terms in the potential (5) have the forms

$$V_d(\rho_{\bar{z}}) = \frac{1}{8}\gamma_z^2(x^2+y^2), \quad V_d(\rho_{\bar{x}}) = \frac{1}{8}\gamma_x^2(z^2+y^2). \qquad (7)$$

The paramagnetic term $\frac{1}{2}\gamma_\alpha l_\alpha$ in Eq. (5) does not depend on the electron coordinates and produces only a shift in the total electron energy. However, the coordinate-dependent diamagnetic term in Eq. (5), having an opposite sign with respect to the Coulomb interactions, will obviously exert a significant effect on the electron motion. It forms a parabolic potential

well that far away from the Coulomb centers confines the electron motion in the direction perpendicular to the field direction. For finite values of the electron coordinates it forms a barrier between the Coulomb centers. Apart from the field strength (γ_α), the relative magnitude of diamagnetic potential with respect to the Coulomb potentials depends (for a given Z) on the impact parameter and the distance $z_0=vt$ [see Eq. (6)].

In Figs. 3(a) and 3(b) we show the three-dimensional (3D) plots of the potential (5) for the parallel and transverse magnetic fields with $\gamma_z=0.2$ and $\gamma_x=0.2$, respectively, for the case $Z=2$, $b=6a_0$, $z_0=30a_0$, and $y=0$. The figures clearly indicate that far enough from the Coulomb centers the diamagnetic term in the potential confines the electronic motion in the direction perpendicular to that of the field. Figure 3(a) shows that in the $\vec{B}\|\vec{v}$ case the diamagnetic term of the interaction even for impact parameters as large as $b=6a_0$ does not form a significant potential barrier between the Coulomb centers to hamper the electron capture process. The electron capture cross section, therefore, does not change significantly with respect to the field-free case. However, for relatively small collision velocities $(E \leqslant 100 \text{ keV}/u)$ the two nuclei stay longer in the region when both the diamagnetic and Coulomb potentials influence the electron motion. The cyclotron motion of the electron in the diamagnetic potential makes the "collision time" even longer thus enhancing the probability of inelastic processes. For the ionized electrons with small kinetic energy, the cyclotron electron motion leads to "trapping" of the electron trajectory in either of the
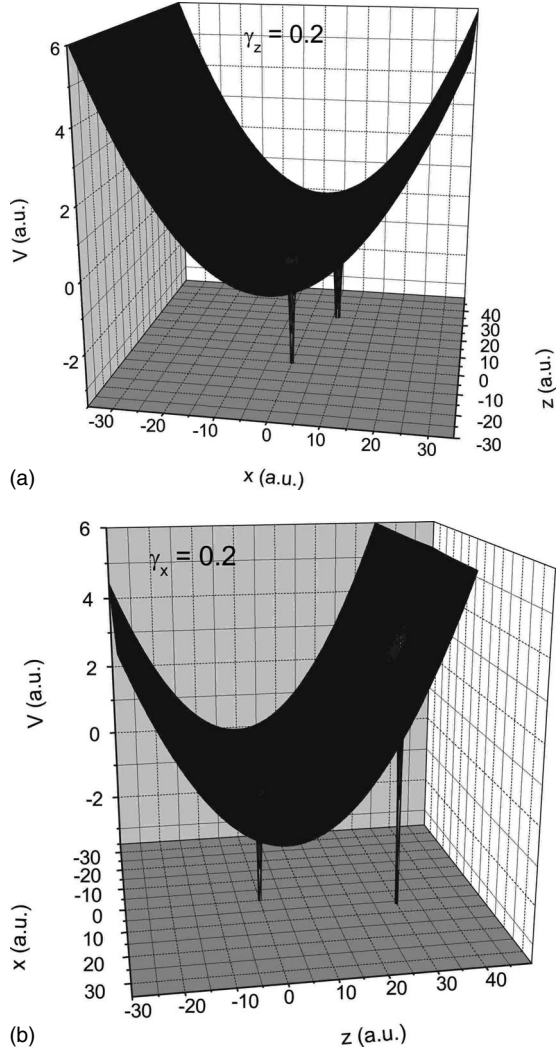
FIG. 3. 3D plots of the potential $V(r;B_\alpha)$ in the parallel [$\alpha=z$, panel (a)] and transverse [$\alpha=x$, panel (b)] magnetic fields for the He^{2+}+H collision system for $l_\alpha=0$, $y=0$, $b=6a_0$, and $z_0=30a_0$.

target or projectile regions for a very long time [15]. During this time the electron bounces on the corresponding Coulomb center and gains energy, which eventually leads to its escape (along the z direction). This also leads to enhancement of ionization cross section in the $\vec{B}\|\vec{v}$ field at low collision energies as observed in Fig. 1(c). The phenomenon of electron trajectory trapping of continuum electrons in the $\vec{B}\|\vec{v}$ field has been discussed in detail in Ref. [15]. The extension of effective collision time and electron bouncing frequency of trapped continuum electrons are obviously proportional γ_z and the calculations of excitation and ionization cross sections with $\gamma_z<0.2$ have indeed shown smaller cross section enhancement in this energy region with respect to the $\gamma_z=0.2$ case.

In the $\vec{B}\perp\vec{v}$ case ($B=B_x$), the diamagnetic parabolic potential well is directed along the x axis [see Fig. 3(b)] and a high potential barrier is formed between the two Coulomb centers. The height of this barrier obviously is proportional to γ_x^2. The electron trajectories that can reach the projectile potential well are severely hampered by this barrier leading

to reduction of electron capture cross section [see Figs. 1(a) and 2(a)] with respect to the unscreened case. This reduction is obviously proportional to the γ_x. The large impact parameters that in the field-free case give dominant contribution to the electron capture process at low energies, now increase the relative dominance of diamagnetic potential with respect to the projectile Coulomb potential [see Eqs. (5) and (6)], leading to stronger reduction of the electron capture cross section at low energies with respect to the field-free case [see Figs. 1(a) and 2(a)]. In addition to the reduction effects of diamagnetic potential barrier, the electron capture cross section is also reduced due to the Lorentz force $\vec{F}_L=\vec{v}\times\vec{B}$, ionizing the loosely bound captured electrons.

The dramatic increase of excitation and ionization cross sections in the case of transverse magnetic field at low energies [see Figs. 1(b), 1(c) and 2(b), 2(c)] is result of the extended collision time due to electron cyclotron motion, and in the case of ionization also due to the trapped electron trajectories around the target and the Lorentz ionization of captured electrons. Electron trajectory trapping near the projectile is not possible in this case since the Lorentz force drives the projectile continuum electrons to escape along the x direction. In the next section we shall analyze the mechanisms of charge exchange, excitation and ionization processes in more detail in terms of time evolution of electron trajectories and associated electron energies.

IV. TIME EVOLUTION OF INELASTIC EVENTS IN A MAGNETIC FIELD

In order to gain a deeper insight into the dynamics of electron capture, excitation, and ionization processes in an external magnetic field, we shall analyze the time evolution of total electron energy relative to the target (E_{et}) and projectile (E_{ep}) in conjunction with the time evolution of the electron distance from the target (r_{et}) and the projectile (r_{ep}). In the case of ionization we shall also look at the time evolution of the electron velocity in the direction of the field. The time evolution of above quantities will be studied for the He^{2+}+H($1s$) collision system at the energy $E=25$ keV/u by following the trajectory up to 10^7 atomic time units. For the purposes of this analysis we shall take only the cases of $\gamma_z=0.2$ and $\gamma_x=0.2$. In order to study the influence of the magnetic field on the electron motion for a given process, we have selected for our calculations such impact parameters for which a specific trajectory leads to a prescribed event (capture, excitation, or ionization) both in the field-free case and when the field is present. When studying the role of different mechanisms of a given process (e.g., excitation or ionization), we have selected over thousand of such trajectories (among the total number of over 10^5 used in total cross section calculations) in order to obtain a meaningful statistics.

A. Electron capture

The time evolution of electron energies E_{et} and E_{ep} and distances r_{et} and r_{ep} for a capture event with $Z=2$, $E=25$ keV/u and $\gamma_z=0.2$ ($\vec{B}\|\vec{v}$) is shown in Fig. 4(a) (for the energies) and Fig. 4(b) (for electron distances). For the se-
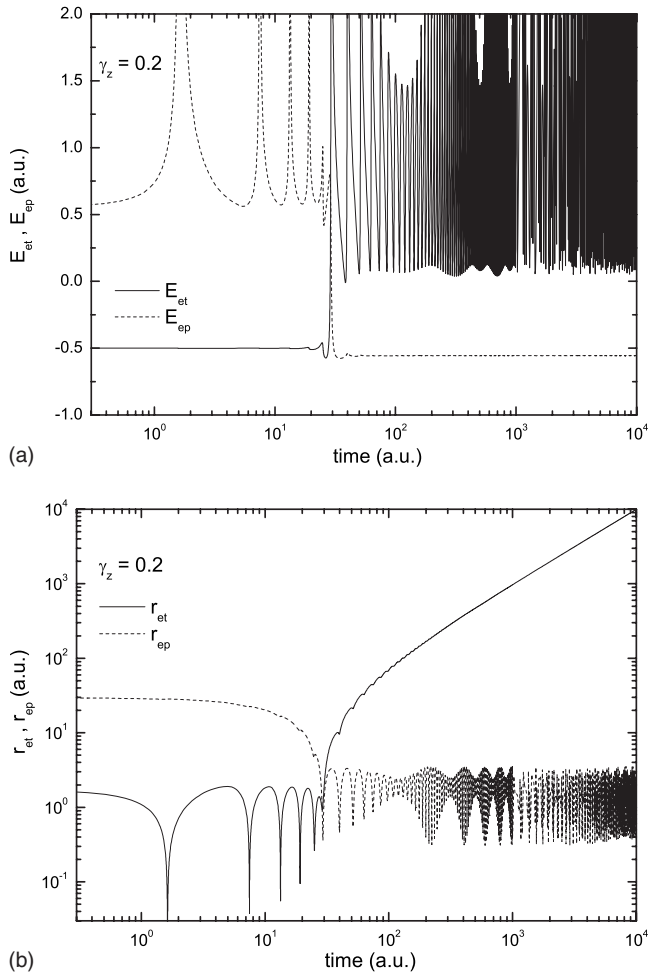
FIG. 4. Time evolution of electron energies E_{et}, E_{ep} (a) and distances r_{et}, r_{ep} (b) for a capture event in the parallel magnetic field of strength $\gamma_z = 0.2$ in $He^{2+}+H$ collision system at $E = 25$ keV$/u$.

FIG. 5. Same as in Fig. 4, but for the transverse magnetic field of strength $\gamma_x = 0.2$.

lected impact parameter and initial distance R_{tp}^0 between the projectile and target nucleus, the electron capture takes place in a relatively small time interval around $t_0 \approx 30$ a.u. during which both E_{et} and E_{ep} are slightly negative, i.e., it moves in the common potential well of the two nuclei, a transient "quasimolecule." This corresponds to the well-known above-barrier electron capture mechanism [17]. The calculation of time evolutions for the same quantities in the field-free case (with the same initial conditions) produces essentially the same picture of their time behavior, but with somewhat shorter duration of the quasimolecular time when the electron resides in the common potential well of the nuclei. The increase of electron residence time in the common potential well would, in principle, increase the capture cross section if the competing ionization mechanisms would not be stronger than the capture. It should be noted in Fig. 4(a) that the binding energy of captured electron remains almost the same as in the initial state $[E_{ep}(t > 40$ a.u.$) = -0.556$ a.u.$]$ and that it is constant. As well known, the parallel magnetic field conserves the total electron energy.

In Fig. 4(b) the electron distances from the target and projectile are shown. In the short time interval around $t_0 \approx 30$ a.u. the electron is close to both target and projectile
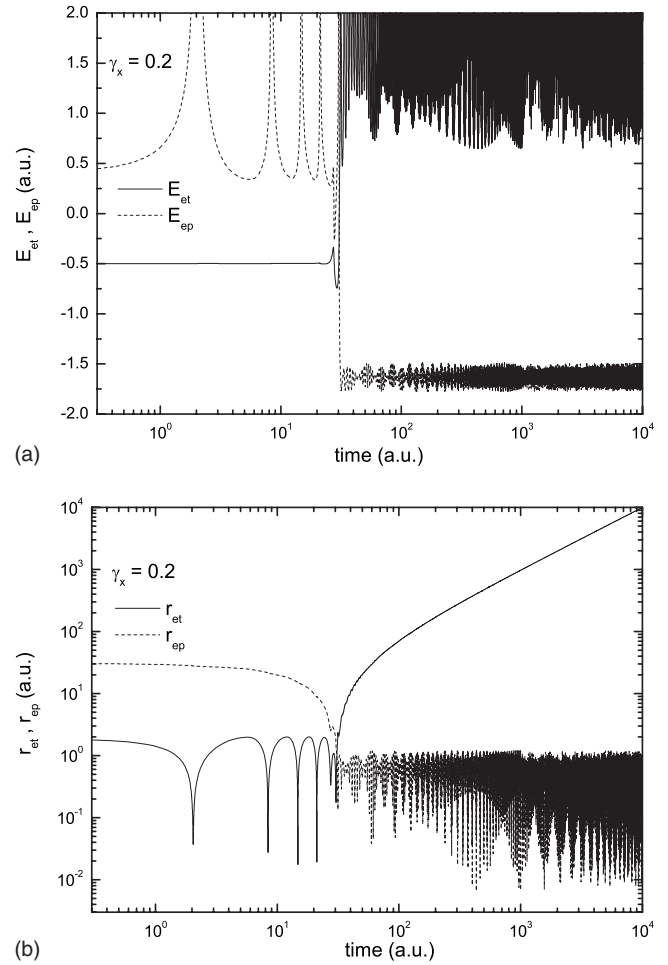
nucleus, indicating that the capture process is indeed governed by an over-barrier transition in the double potential well of the nuclei. Figure 4(b) also shows that captured electron around the moving projectile experiences two types of periodic motion: a high-frequency periodic motion around the nucleus and a low-frequency cyclotron motion due to its translational motion with the projectile in the external magnetic field.

The time evolutions of electron energies E_{et} and E_{ep} and distances r_{et} and r_{ep} for a capture event in the transverse magnetic field of strength $\gamma_x = 0.2$ (with the same collision parameters and initial conditions and as in the case of parallel field) are shown in Fig. 5(a) (for the energies) and Fig. 5(b) (for the distances). The time evolution of these quantities is similar to that in the case of parallel magnetic field except for two important differences: the binding energy of captured electron is no more a constant of motion and the duration of quasimolecular time is longer than in the case of $\vec{B} \| \vec{v}$ field. The total electron energy of captured electron oscillates with an atomic frequency and amplitudes of these oscillations are determined by the cyclotron oscillations of the electron due to the magnetic field. The electron distance r_{ep} exerts similar oscillations [cf. Fig. 5(b)]. It should be noted that the mean electron binding energy of captured elec-

tron in this case is about -1.57 a.u., i.e., much larger than that of captured electron in the case of $\vec{B} \parallel \vec{v}$ field. Due to the Lorentz ionization, only the captured electrons with large binding energy remain bound. The longer electron residence time in the common potential well of the nuclei in the case of $\vec{B} \perp \vec{v}$ field does not lead to an increase of capture probability but rather to an increase of the probability of competing ionization process.

B. Excitation

By analyzing a large number of trajectories leading to target excitation in the $He^{2+}+H(1s)$ system at $E=25$ keV/u and for $\gamma_z=0.2$, we have found that the main excitation mechanism in the case of $\vec{B} \parallel \vec{v}$ field is the direct energy transfer between the projectile and target electron (direct excitation), which accounts for about 70% of the total excitation events. However, a significant number (about 30%) of trajectories were found for which the electron distances from the nuclei were close to each other for a considerable time. In absence of the field, such trajectories would lead to elastic scattering. Such trajectories lead to a "field assisted" excitation and are responsible for the cross section increase observed in Fig. 1(b) at low energies. The electron energies and distances relative to the target and the projectile for a trajectory leading to direct excitation are shown in Figs. 6(a) and 6(b), respectively.

In the case of transverse magnetic field with strength $\gamma_x=0.2$, the analysis of a large number of trajectories (for the same collision system and energy) leading to excitation has shown that the predominant part of excitation events (70%) are due to trajectories for which the electron transiently resides in the common potential well of the two nuclei (where both E_{et} and E_{ep} are negative). The direct excitation [when $E_{et}<0$ and $E_{ep}>0$ during the entire time evolution, or when E_{et} (E_{ep}) becomes positive (negative) for a time shorter than its atomic period] in this case accounts for the remaining 30% of the trajectories. We should note that in the absence of external magnetic field all the trajectories involved in the indirect excitation mechanism lead to electron capture. Thus, the increase of the excitation cross section in the $\vec{B} \perp \vec{v}$ field at low energies is at expense of the reduction of electron capture cross section. As we shall see in the next subsection, further reduction of the electron capture cross section in this energy region is due to the similar indirect ionization mechanism.

The relative importance of direct and indirect excitation mechanisms will, of course, change with changing the collision velocity. Thus, with increasing the collision energy, the role of direct excitation mechanism is expected to increase since the collision time becomes shorter and so will be the electron residence time in the double potential well of the nuclei.

C. Ionization

The CTMC dynamics of the ionization process in a $\vec{B} \parallel \vec{v}$ field has been studied in detail in Ref. [15] on the ion—
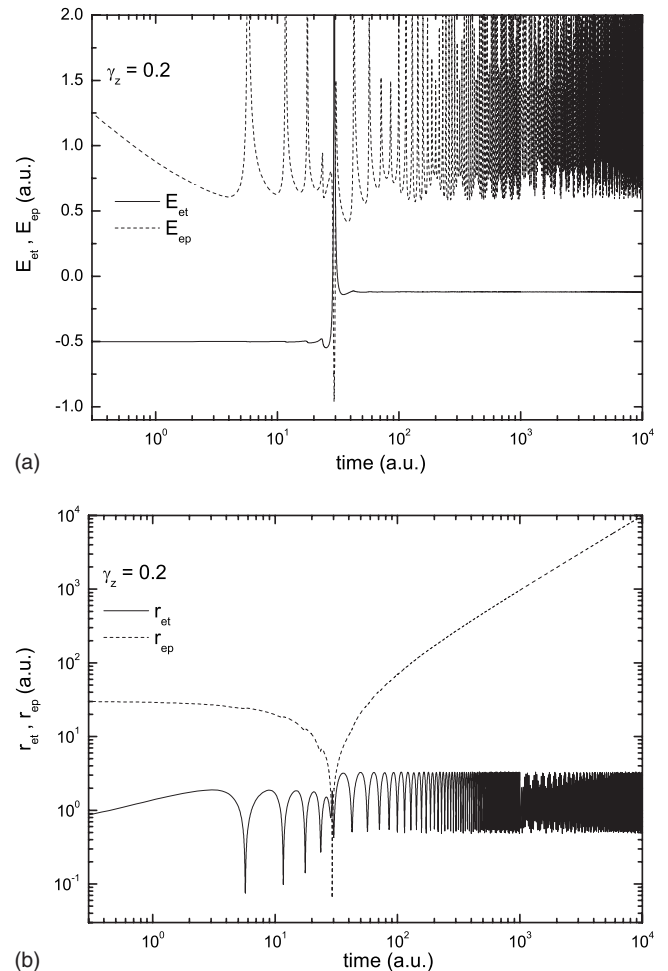

FIG. 6. Time evolution of electron energies E_{et}, E_{ep} (a) and distances r_{et}, r_{ep} (b) for an excitation event in the parallel magnetic field of strength $\gamma_z=0.2$ in $He^{2+}+H$ collision system at $E=25$ keV/u.

Rydberg atom collision system. It was found that three main mechanisms contribute to the ionization process: direct (or prompt) ejection of the electron to the continuum, long-time trapping of low-energy continuum electrons in the target and projectile regions, and their ultimate escape along the field direction and the saddle-point ionization mechanism [20]. Of these three ionization mechanisms the most effective was found to be the trapped electron mechanism, whereas the weakest one is the saddle-point mechanism. The conclusions of Ref. [15] have been confirmed also in the trajectory analysis of ionization events in present calculations for the $He^{2+}+H$ collision system at 25 keV/u in a $\vec{B} \parallel \vec{v}$ field with strength $\gamma_z=0.2$. Since the trajectory behavior for the $\vec{B} \parallel \vec{v}$ field case was thoroughly discussed in Ref. [15] we shall omit detailed discussion of these mechanisms in the present paper and show only the time evolution of electron energies and distances relative to the target and projectile for one trajectory leading to a long-time trapping of a continuum electron around the projectile and its escape [Figs. 7(a) and 7(b), respectively]. As the continuum electron energy for this specific ionization event is very small, the trapping time is rather long (from about 30 a.u. to about 10^6 a.u.). During all this
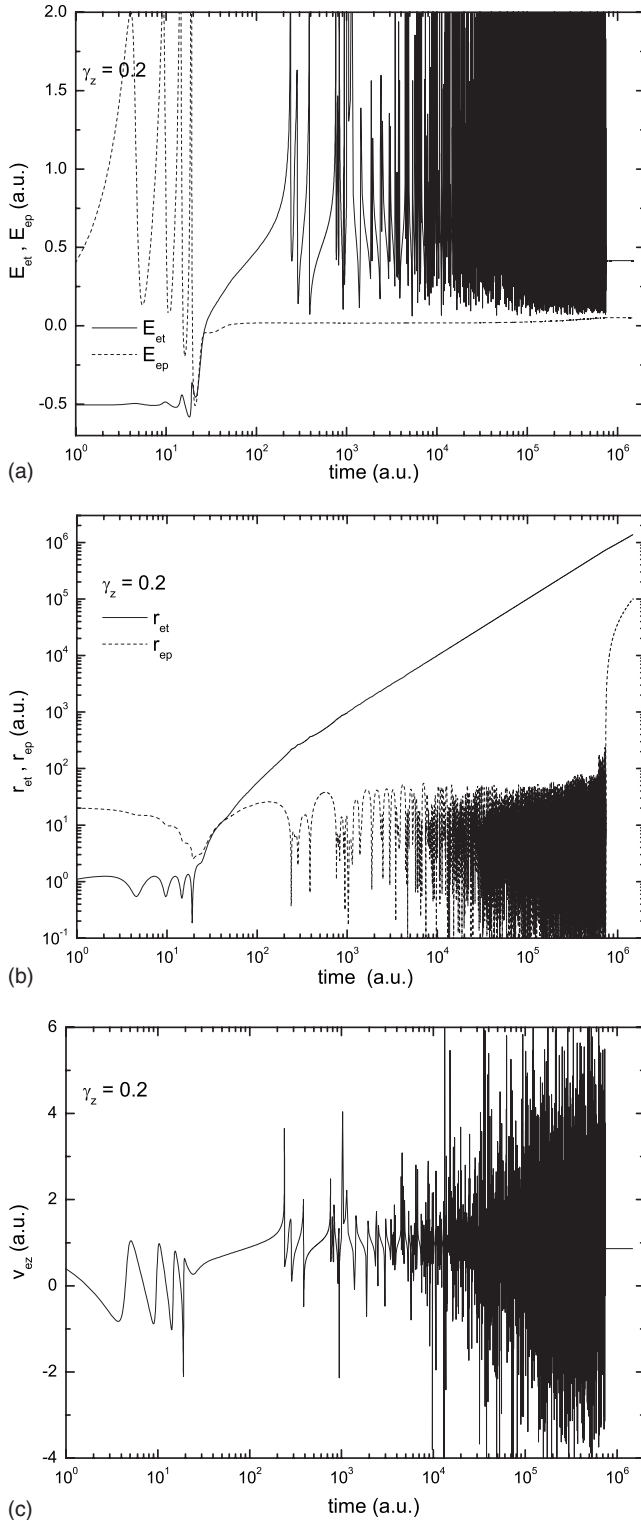
FIG. 7. Time evolution of electron energies E_{et}, E_{ep} (a), electron distances r_{et}, r_{ep} (b) and electron velocity component v_{ez} (c) of an ionization event in the parallel magnetic field of strength $\gamma_z = 0.2$ in $He^{2+} + H$ collision system at $E = 25$ keV/u with electron trajectory trapped in the projectile region.

time the ionized electron remains in the projectile region [see Fig. 7(b)] and at the end of this time interval it exchanges energy with the projectile [whereby its energy is increased, see Fig. 7(a)] and escapes along the z direction. Figure 7(c)

shows the behavior of the electron velocity component in the field direction v_{ez}. During the trapping time, v_{ez} oscillates around certain mean value (in both the positive and negative direction of z) and becomes constant when the electron leaves the trapping region.

By analyzing about 1000 ionization trajectories we have found that the direct ionization accounts for 22%, the trapped trajectory mechanism accounts for 74%, and the saddle point mechanism accounts for 4% of the total number of ionization events. About 40% of trapped trajectories were trapped in the target region and about 60% in the projectile region.

In the case of transverse magnetic field the electron is ionized by three mechanisms: direct ionization (prompt ejection to the continuum and escape from the target field), trapping of the continuum electron in the target region and consecutive escape from that region in the field (x) direction, and Lorentz ionization of captured electron. As we mentioned earlier, due to the Lorentz force, trapping of a continuum electron in the projectile region cannot take place. It is also obvious that the condition for the saddle point ionization mechanism can never be fulfilled in the transverse magnetic field (even approximately, as in the case of the $\vec{B} \| \vec{v}$ field). The time evolutions of electron energies and distances relative to the target and projectile, as well as of the electron velocity component in the field direction, v_{ex}, for trajectories representative for the above mentioned three mechanisms in the $\vec{B} \perp \vec{v}$ field are shown in Figs. 8, 9, and 10, respectively.

The prompt character of direct ionization mechanism is evident from Fig. 8: the energy exchange between the projectile and target electron brings the latter in the continuum [Fig. 8(a)] and its departure from the target nucleus and the projectile starts immediately after its ejection to the continuum [Fig. 8(b)].

Figure 9 illustrates the ionization mechanism with electron trajectory trapping. Although the energy of ejected electron is 0.5 a.u. [see Fig. 9(a)], the electron is for a long time interval [$t \sim 40 - 10^4$ a.u., cf. Fig. 9(b)] still in the target region where its motion is affected by the interaction with both the target nucleus and the magnetic field. Its velocity component in the direction of the field becomes constant only when it escapes this region [Fig. 9(c)].

The Lorentz ionization mechanism is illustrated in Fig. 10. The electron is captured by the projectile at about $t \approx 20$ a.u. [Figs. 10(a) and 10(b)], then it is excited by the Lorentz force at $t \approx 2500$ a.u. and finally ionized at $t \approx 2 \times 10^4$ a.u. in the negative x direction [see Fig. 10(c)]. After its ejection in the continuum, the electron moves along the x direction which is reflected in the change of the slope of the distance r_{et} [cf. Fig. 10(b)] and the constant value of v_{ex} (of -0.1075 a.u.). By analyzing about 2000 ionization trajectories we have found that the direct, trapped trajectory and Lorentz ionization mechanisms contribute respectively by about 14, 82, and 4 % to the total ionization.

V. ENERGY DISTRIBUTION OF CAPTURED, EXCITED, AND IONIZED ELECTRONS

The distributions $f(E_{et})$, $f(E_{ep})$, $f(v_{ez})$, and $f(v_{ex})$ that will be discussed in the present section are all defined as
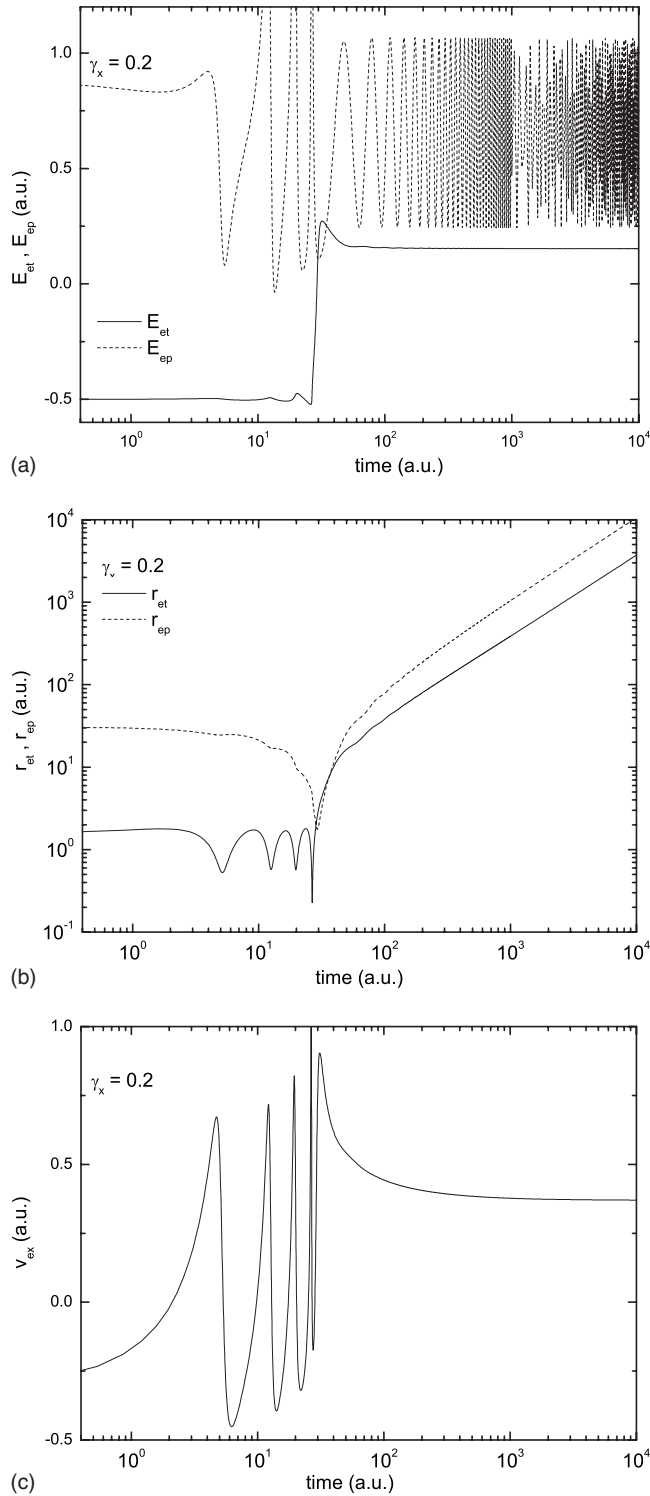
FIG. 8. Time evolution of electron energies E_{et}, E_{ep} (a), electron distances r_{et}, r_{ep} (b) and electron velocity component v_{ex} (c) of a direct ionization event in the transverse magnetic field of strength $\gamma_z = 0.2$ in He^{2+}+H collision system at $E = 25$ keV/u.

$$f(a) = \frac{N(a)}{\int N(a)da}, \quad (8)$$

where $N(a)$ is the number of events with the quantity a having values between a and $a+\Delta a$, and Δa is sufficiently small.
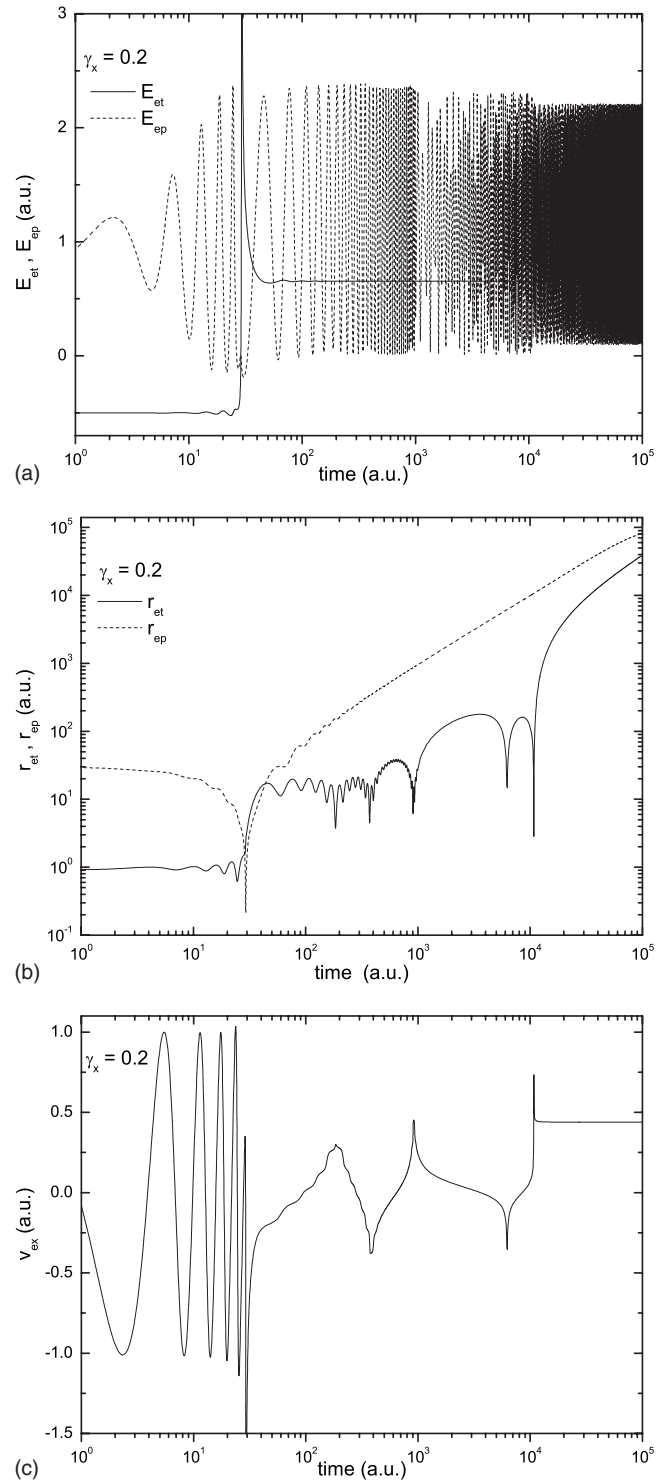

FIG. 9. Same as in Fig. 8, but for an ionization event with electron trajectory trapping in the target region.

A. Electron capture

The conservation of total electron energy of captured electrons in the parallel magnetic field and its nonconservation in the transverse magnetic field, as demonstrated in Figs. 4(a) and 4(b), respectively, should lead to quite different classical energy distributions of captured electrons in these two cases. Figure 11 shows such distributions for $Z=2$, γ
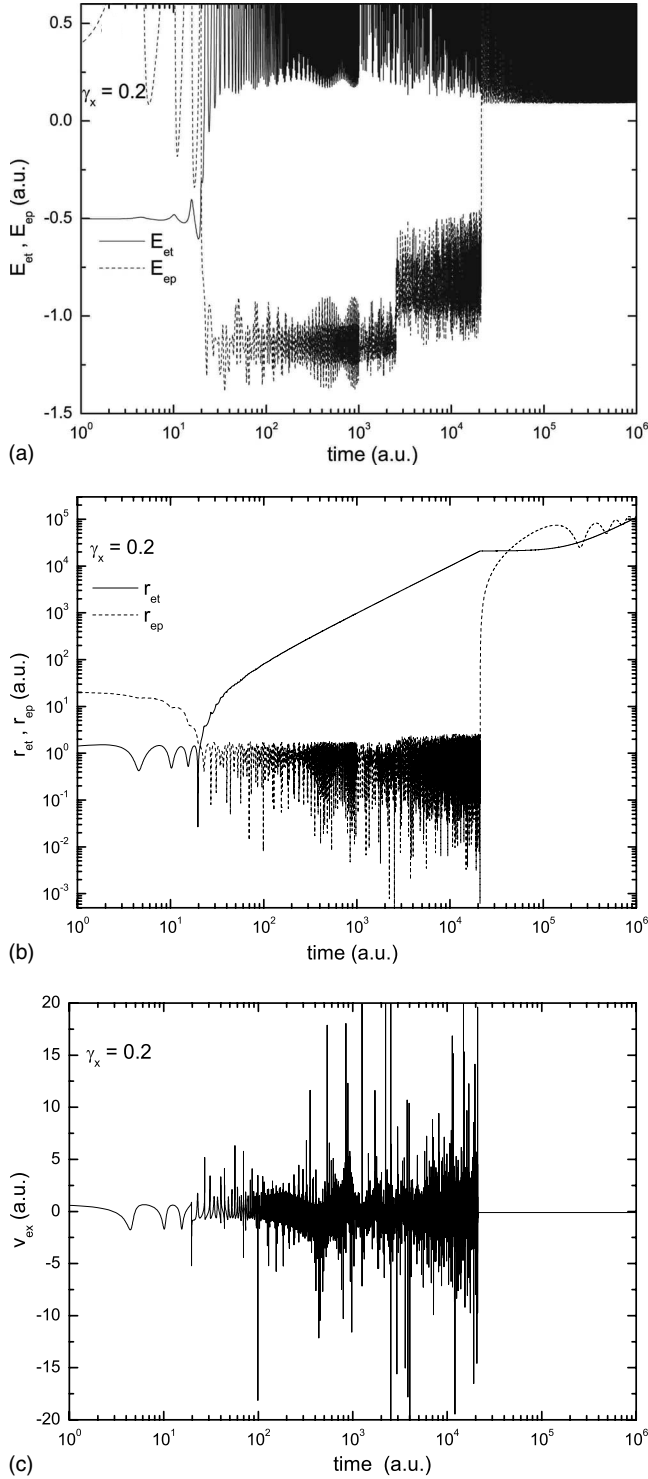
FIG. 10. Same as in Fig. 8, but for Lorentz ionization of a captured electron.

It should be noted that the energy distribution is peaked around −0.5 a.u., corresponding to the $n=2$ level in He$^+$ which is resonant in energy with the initial state.

In the case of a transverse magnetic field the energy distribution of captured electrons differs drastically from that in the field-free case [see Fig. 11(b)]. The distribution in the transverse magnetic field has a maximum at $E \approx -1$ a.u. ($n_{eff} \approx 1.4$) indicating that the capture to states with smaller binding energy is being severely reduced with respect to the field-free case. This is an effect of the Lorentz ionization of high-n captured electrons.

B. Excitation and ionization

The classical energy distributions of excited ($-0.22 < E_{et} < 0$) and ejected ($E_{et} > 0$) electrons in reactions (2) and (3) with $Z=2$ in a parallel ($\gamma_z = 0.2$) and transverse ($\gamma_x = 0.2$) magnetic field at the collision energy of 25 keV/u are shown in Figs. 12(a) and 12(b), respectively, together with the corresponding field-free distribution. The energy distribution of excited electrons in the $\vec{B} \| \vec{v}$ field [Fig. 12(a)] is similar to that of the field-free case. In both cases most of the excitation events populate the low-lying states, which is another indication of the dominance of direct excitation mechanism in both cases.

The energy distributions of ionized electrons in the $\vec{B} \| \vec{v}$ field case is, however, significantly different than that in the field-free case. The zero-energy peak of the field-free distribution of ionized electrons is significantly reduced in the parallel magnetic field since the trajectories of majority of these electrons are trapped in the target or projectile regions and then ejected with a larger energy [see Fig. 7(a)]. The trapped trajectory electrons are also responsible for the broadening of energy distribution of ionized electrons in the field case.

The energy distributions of excited and ionized electrons in the $\vec{B} \perp \vec{v}$ field are markedly different from those of the field-free case [see Fig. 12(b)]. The majority of excited electrons in the transverse field case have small binding energies, an indication that the excitation in this case proceeds dominantly via the transient formation of a common potential well of the nuclei, as discussed in Sec. IV B. The observed decrease of zero-energy peak of the distribution of ionized electrons (with respect to that in the field-free case) and its broadening is related, as in the case of $\vec{B} \| \vec{v}$ field, to the trapped trajectory electrons. The Lorentz ionization of captured electrons is an additional source of high-energy electrons in the distribution. The broad peak in the distribution of ionized electrons around $E_{et} = 0.5$ a.u. is related to the electrons captured to the projectile continuum (ECC peak) [17].

We note that the observed patterns of the energy distributions of excited and ionized electrons in the $\vec{B} \| \vec{v}$ and $\vec{B} \perp \vec{v}$ fields remain the same with varying the collision energy and the strength of magnetic field. However, some of their features are more or less pronounced. For example, for $\gamma_x = 0.1$ and $E = 25$ keV/u, the ECC peak is much more pronounced than in the $\gamma_x = 0.2$ case since in the weaker field the trapped trajectory ionization mechanism is also weaker.
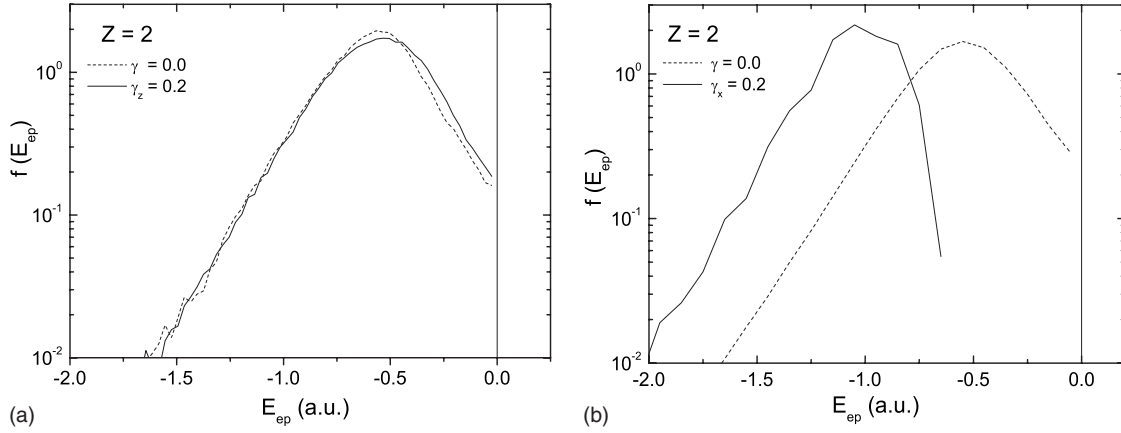
=0.0, $\gamma_z = 0.2$ [Fig. 11(a)] and $Z=2$, $\gamma=0.0$, $\gamma_x=0.2$ [Fig. 11(b)] for collision energies of $E=25$ keV/u. From Fig. 11(a) it can be observed that the field-free and $\gamma_Z=0.2$ distributions are close to each other. This indicates that by using the classical-quantum energy correspondence principle and binning rules as in, for instance, in Ref. [21] one can obtain distributions of captured electrons over the final state principal quantum numbers n close to those in the field-free case.

FIG. 11. Energy distributions of captured electrons in He^{2+}+H collision at $E=25$ keV/u in the parallel magnetic field of strength γ_z =0.2 (a) and transverse magnetic field of strength γ_x=0.2 (b) compared with the corresponding distribution in the field-free case (γ=0.0).

C. Velocity distributions of emitted electrons in the field direction

A further insight in the ionization process in the presence of an external magnetic field is provided by the velocity distributions of emitted electrons, particularly of their component in the field direction. In Fig. 13 we show the distribution of the v_z velocity component of the emitted electrons in the $\vec{B} \| \vec{v}$ field (with strength γ_z=0.2) for the He^{2+}+H collision at 25 keV/u [panel (a)] and 100 keV/u [panel (b)] together with its distribution in the field-free case. Two distinct features can be noted in these figures that are introduced by the field in the ejected electron distribution in the z direction: (i) strong enhancement of backward ejected electrons when the field is present and (ii) appearance of dips in the distribution when the z component of electron velocity is equal to zero and to the projectile velocity v_p [v_z=1 in Fig. 13(a) and v_z=2 in Fig. 13(b)]. The dips in the v_z distribution at $v_z \approx 0$ and $v_z - v_p \approx 0$ are related to the absence of the Lorentz force component in the field direction and the "capture" of these zero-(relative) velocity continuum electrons by the Coulomb field of the target and projectile, respectively. Since in the parallel (B_z) field case the v_z-component is con-

served, while the other two velocity components oscillate with an average value close to zero for low collision energies (as found in detailed trajectory calculations), the condition $v_e = v_p/Z$ for the "saddle point" ionization mechanism [20] is well fulfilled for the case in Fig. 13(a) ($v_z \approx v_e = v_p$, Z=2) where the maximum of the v_z-velocity distribution is observed at $v_z \approx 0.5$ a.u. For the 100 keV/u energy case [Fig. 13(b)], however, the peak of the distribution is below the value $v_z \approx 1.0$, indicating that the contribution of other two velocity components to v_e is appreciable. We note that the same features of v_z distributions in the $\vec{B} \| \vec{v}$ field were found also in Ref. [15] when studying the ionization in ion—Rydberg atom collisions.

The velocity distribution of ejected electrons in the x-direction for the same collision system in a transverse magnetic field with strength γ_x=0.2 is shown in Figs. 14(a) and 14(b) for the energies of 25 and 100 keV/u, respectively. The x component of ionized electrons velocity in the field-free case is also shown for comparison. In both the field and field-free cases the v_x distributions are symmetric with respect to v_x=0. In the field-free case the v_x distribution for the energy of 25 keV/u [Fig. 14(a)] exhibits a two-component structure; the component that broadens the high-velocity part
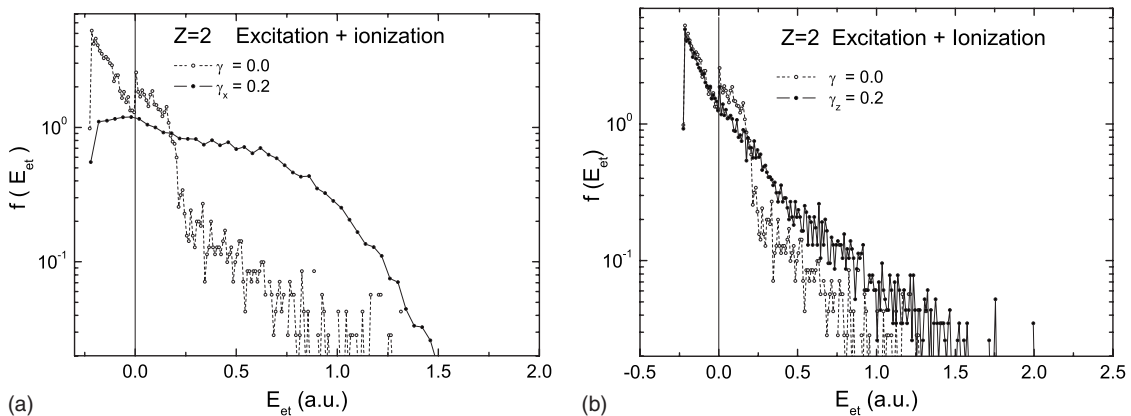

FIG. 12. Energy distributions of excited ($E_{et}<0$) and ionized ($E_{et}>0$) electrons in He^{2+}+H collision at $E=25$ keV/u in the parallel magnetic field of strength γ_z=0.2 (a) and transverse magnetic field of strength γ_x=0.2 (b) compared with the corresponding distribution in the field-free case (γ=0.0).
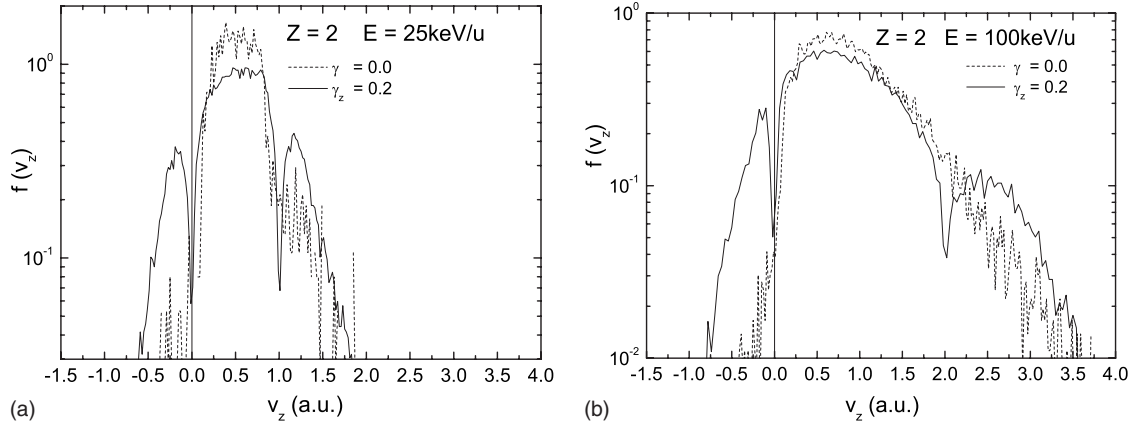
FIG. 13. Electron velocity distributions of ionized electrons in He^{2+}+H collision in a parallel magnetic field of strength γ_z=0.2 ejected in the field direction, for collision energies of 25 keV/u (a) and 100 keV/u (b). Corresponding distributions in the field-free case (γ =0.0) are also shown.

of the distribution is due to the ECC electrons. This component in the field-free distribution disappears at 100 keV/u [Fig. 14(b)] as the capture to the continuum is negligible at this energy. Two v_x distributions in the presence of the $\vec{B} \perp \vec{v}$ field are significantly broader in the low-velocity part of the spectrum than in the field-free case, particularly for the E =25 keV/u collision energy, which is an effect of the trapped trajectory electrons. The dip in the v_x distribution at v_x=0, more pronounced for E=100 keV/u, is a result of the field-assisted "capture" of the zero-energy continuum electrons in the atomic region. The electron velocity component $v_\perp$ in the direction perpendicular to the field has its maximum at $v_\perp \approx 0$.

VI. CONCLUSIONS

In the present work we have studied the electron capture, excitation and ionization processes of a fully stripped ion colliding with the ground-state hydrogen atom in external magnetic fields $B \leqslant 0.2B_0$ parallel and perpendicular to the projectile velocity vector by using the CTMC method. The total cross sections of these processes were calculated in the energy range from 25 keV/u to 1000 keV/u for ions with Z=2 and 6, while the investigation of time evolution of elec-

tron capture, excitation, and ionization dynamics, as well as of energy distributions of captured, excited and ionized electrons was done for the Z=2 ion only and a selected number of collision energies. The general conclusions of the present study can be summarized as follows.

(i) In the considered energy range, the parallel magnetic field has an insignificant effect on the total electron capture cross section, it leads to a moderate increase of the total excitation and ionization cross sections in the energy range $E/Z \leqslant 100$ keV/u and $E/Z \leqslant 50$ keV/u, respectively, compared to the corresponding field-free cross sections. The transverse magnetic field leads to a significant reduction of the total electron capture cross section in the entire energy range investigated. This reduction increases with increasing the field strength and is result of the formation of an effective diamagnetic potential barrier between the Coulomb potential wells of the nuclei, as well as of the Lorentz ionization of weakly bound captured electrons. The total excitation and ionization cross sections in the energy regions below $E/Z \leqslant 100$ keV/u and $E/Z \leqslant 50$ keV/u, respectively, show a dramatic increase with increasing both the field strength and Z, associated mainly with the indirect mechanisms for these processes.

(ii) The analysis of time evolution of a large number (over 1000) trajectories for each of considered processes has re-
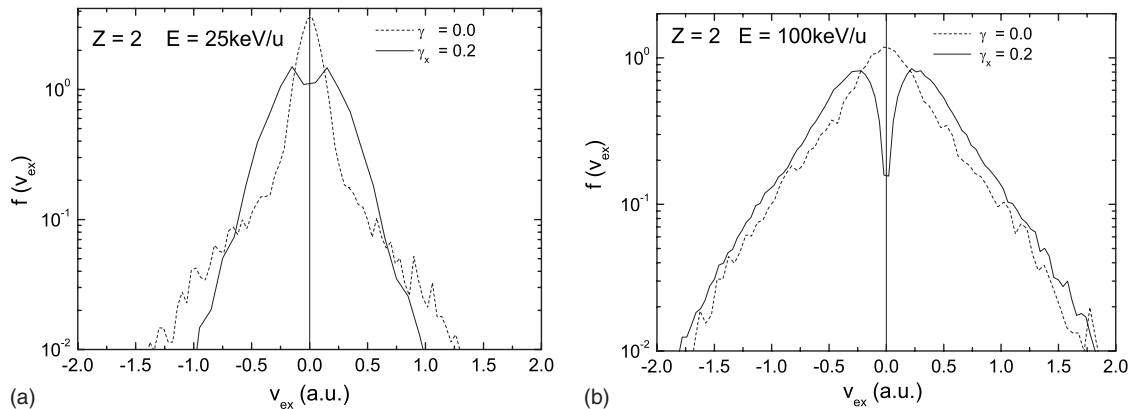

FIG. 14. Same as in Fig. 13, but for the transverse magnetic field of strength γ_x=0.2.

vealed that the magnetic field extends the effective collision time at low collision energies, thus enhancing the role of indirect transition mechanisms, particularly for excitation and ionization. The transient formation of a double potential well for the electron motion at low collision energies, in conjunction with the electron cyclotron motion, facilitates the excitation process, particularly in the transverse magnetic field. Similarly, the trajectory trapping of continuum electrons in the atomic regions due to its cyclotron motion becomes the main ionization mechanism in both the parallel and transverse magnetic field.

(iii) The classical energy distributions of captured, excited and ionized electrons in the parallel magnetic field (that conserves the total electron energy) remain close to those in the field-free case. Only the energy distribution of ionized electrons is significantly broadened with respect to the field-free case due to the contribution of trapped continuum electrons. However, in the transverse magnetic field the energy distributions of captured, excited, and ionized electrons become considerably different than in the field-free case. The weakly bound captured electrons are eliminated from the energy spectrum of captured electron due to their Lorentz ionization. This same process, however, increases the high-energy part of energy distribution of ionized electrons with respect to the field-free case. The increase of the residence time in the double potential well of the nuclei in the case of the trans-verse field enhances the population of weakly bound excited electrons. The distributions of velocity components of ionized electrons in the field direction both in the parallel and transverse magnetic field show distinct differences with respect to the field-free case. In the parallel magnetic field case, the v_z distribution shows a significantly increased fraction of backward emitted electrons as result of the continuum electron trajectory trapping. Characteristic dips appear in this distribution when v_z is close to zero in the target or projectile reference frame caused by the field-assisted "capture" of these continuum electrons in the field corresponding Coulomb center. In the case of transverse magnetic field the v_x distribution is fully symmetric with respect to $v_x=0$, where it exhibits a dip, absent in the field-free case.

[1] R. H. Garstang, Rep. Prog. Phys. **40**, 105 (1977).

[2] W. Rosner, G. Wunner, H. Herold, and H. Ruder, J. Phys. B **17**, 29 (1984).

[3] D. M. Larsen, Phys. Rev. A **25**, 1295 (1982).

[4] G. Wunner, H. Herold, and H. Ruder, Phys. Lett. **88A**, 344 (1982).

[5] U. Wille, Phys. Rev. A **38**, 3210 (1988).

[6] S. Bivona, B. Spagnolo, and G. Ferrante, J. Phys. B **17**, 1093 (1984).

[7] S. Bivona and M. R. C. McDowell, J. Phys. B **20**, 1541 (1987).

[8] U. Wille, Phys. Lett. A **125**, 52 (1987).

[9] S. Suzuki, N. Shimakura, and M. Kimura, J. Phys. B **29**, 1063 (1996).

[10] T. P. Grosdanov and M. R. C. McDowell, J. Phys. B **18**, 921 (1985).

[11] S. Bradenbrink, E. Y. Sidky, Z. Roller-Lutz, and H. O. Lutz, J. Phys. B **30**, L161 (1997).

[12] S. Bradenbrink, E. Y. Sidky, Z. Roller-Lutz, H. Reihl, and H. O. Lutz, Phys. Rev. A **55**, 4290 (1997).

[13] U. Fano, F. Robicheaux, and A. R. P. Rau, Phys. Rev. A **37**, 3655 (1988).

[14] E. A. Solov'ev, Sov. Phys. JETP **55**, 1017 (1982).

[15] S. Bradenbrink, H. Reihl, Z. Roller-Lutz, and H. O. Lutz, J. Phys. B **30**, 5819 (1997).

[16] V. S. Popov, B. M. Karnakov, and V. D. Mur, JETP **88**, 902 (1999).

[17] R. K. Janev, L. P. Presnyakov, and V. P. Shevelko, *Physics of Highly Charged Ions* (Springer, Berlin, 1985).

[18] R. Abrines and I. C. Percival, Proc. Phys. Soc. London **88**, 873 (1966).

[19] R. E. Olson and A. Salop, Phys. Rev. A **16**, 531 (1977).

[20] R. E. Olson, Phys. Rev. A **27**, 1871 (1983).

[21] R. L. Becker and A. D. MacKellar, J. Phys. B **17**, 3923 (1984).